Supporting Information

Twist-angle Dependent Optoelectronics in few-layer Transition-Metal Dichalcogenides Heterostructure

Woosuk Choi[1†], Imtisal Akhtar[1†], Malik Abdul Rehman[1†], Minwook Kim[1], Dongwoon Kang[1], Jongwan Jung[1], Yoon Myung[1], Jungcheol Kim[3], Hyeonsik Cheong[3], Yongho Seo[1,2*]

[1]Department of Nanotechnology and Advanced Material Engineering, Sejong University, Seoul, 05006, Korea

[2] Graphene Research Institute and HMC, Sejong University, Seoul, 05006, Korea

[3] Department of Physics, Sogang University, Seoul 04107, Korea

[†]These authors contributed equally to this work

[*]Corresponding author

E-mail: yseo@sejong.ac.kr, Tel.:+82-2-3408-3689

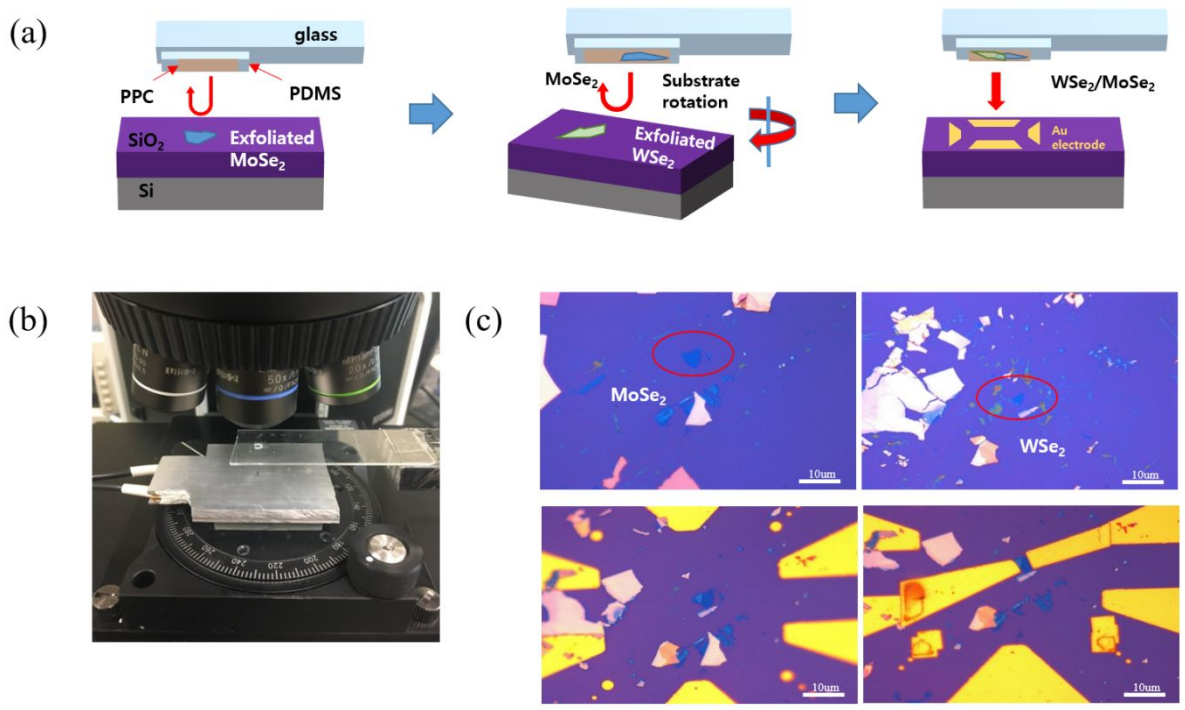

Figure S1 Sample fabrication process of $WSe_2/MoSe_2$ heterostructure p-n junction. (a) Schematic illustration of a pick-up transfer process. (b) Photograph of transfer setup composed of an optical microscope and heater stage. (c) Optical micrographs of WSe_2 and $MoSe_2$ transferred on SiO_2.

Pick-up process was applied for fabricating $WSe_2/MoSe_2$ heterostructure. First the WSe_2 and $MoSe_2$ thin layers on SiO_2 were prepared individually using conventional micromechanical exfoliation method. A thin polypropylene carbonate (PPC) film was attached onto a polydimethylsiloxane (PDMS) stamp with a glass-slide as shown in Fig. S1(a). After the crystal orientation was confirmed, stamping it on the SiO_2, $MoSe_2$ was picked up onto PPC using an optical microscope as shown in Figure S1 (b). Then, it was stamped again, to pick up the WSe_2, while adjusting the twist angle. Then, the $WSe_2/MoSe_2$ heterostructure on the PPC was transferred onto another SiO_2 substrate by heating at 100 °C, on which large electrodes were previously deposited. PPC was removed using chloroform and the large electrodes were connected to WSe_2 and $MoSe_2$ by small electrodes using e-beam lithography as shown in Figure S1 (c).

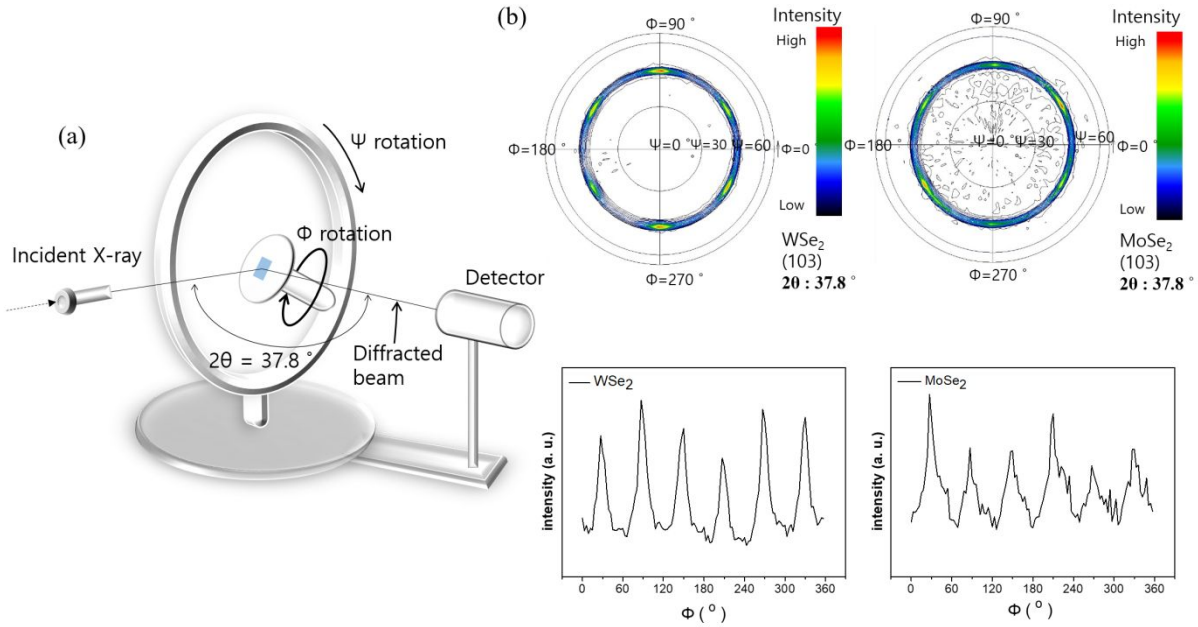

Figure S2 HR-XRD data of disarranged sample. (a) Schematic drawing of Φ and Ψ scan of HR-XRD, with 2θ=37.8° fixed. (b) HR-XRD data of WSe_2 and $MoSe_2$ were plotted in pole figure.

High-resolution x-ray diffraction (HR-XRD) was used to determine the crystal orientation of WSe_2 and $MoSe_2$. Figure S2(a) shows how the crystal orientation of samples were measured with Φ and Ψ scan. It is well-known that WSe_2 (JCPDS Card No. 87-2418) and $MoSe_2$ (JCPDS Card No. 77-1715) have strong XRD peaks at 2θ=37.8° for the crystal plane (103). Figure S2(b) shows HR-XRD pole figure data of disarranged samples, where the crystal orientations of WSe_2 and $MoSe_2$ flakes were slightly disordered. The intensity value was much smaller than that of the ordered sample, and the peaks were not sharp and spread widely.

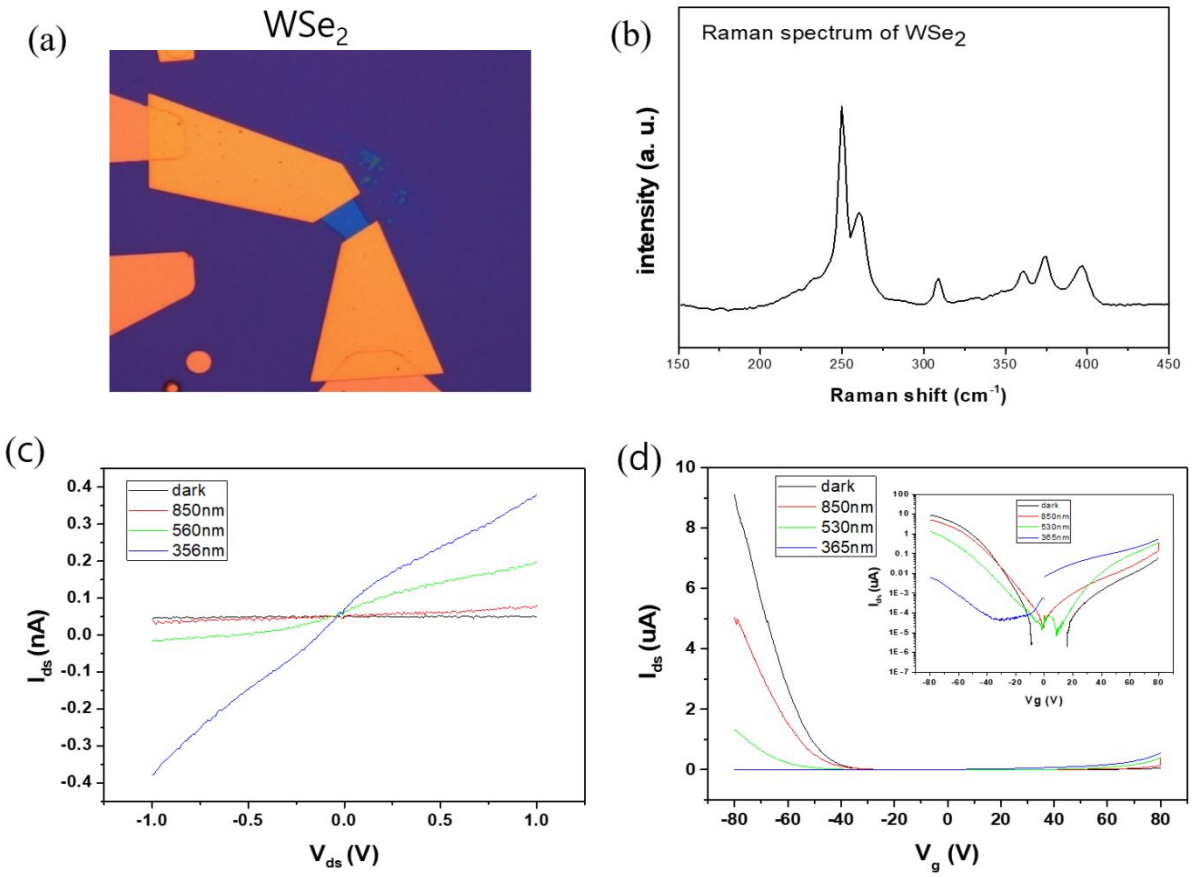

Figure S3 The optoelectronic data of few layer WSe_2 based FET. (a) The optical microscopic image, (b) Raman spectrum, (c) I-V curve at different illumination conditions, and (d) transfer curves depending on the back-gate voltage (@ V_{ds} = 1 V). The inset is a semi-log plot of the same data.

To understand the characteristics of few layer WSe_2, a FET device with WSe_2 single crystal was fabricated, as shown in Fig. S3(a). The thickness with 4 layers was confirmed from Raman spectrum, as shown in Fig. S3(b). The I-V curves were measured under the dark, 850 nm, 530 nm, and 365 nm illumination conditions, as shown in Fig. S3(c). Photocurrent of WSe_2 was increased as the photon energy was increased. The current as a function of the back gate voltage was measured to confirm that WSe_2 was p-type as shown in Fig. S3(d), where V_{ds} was set to 1 V.

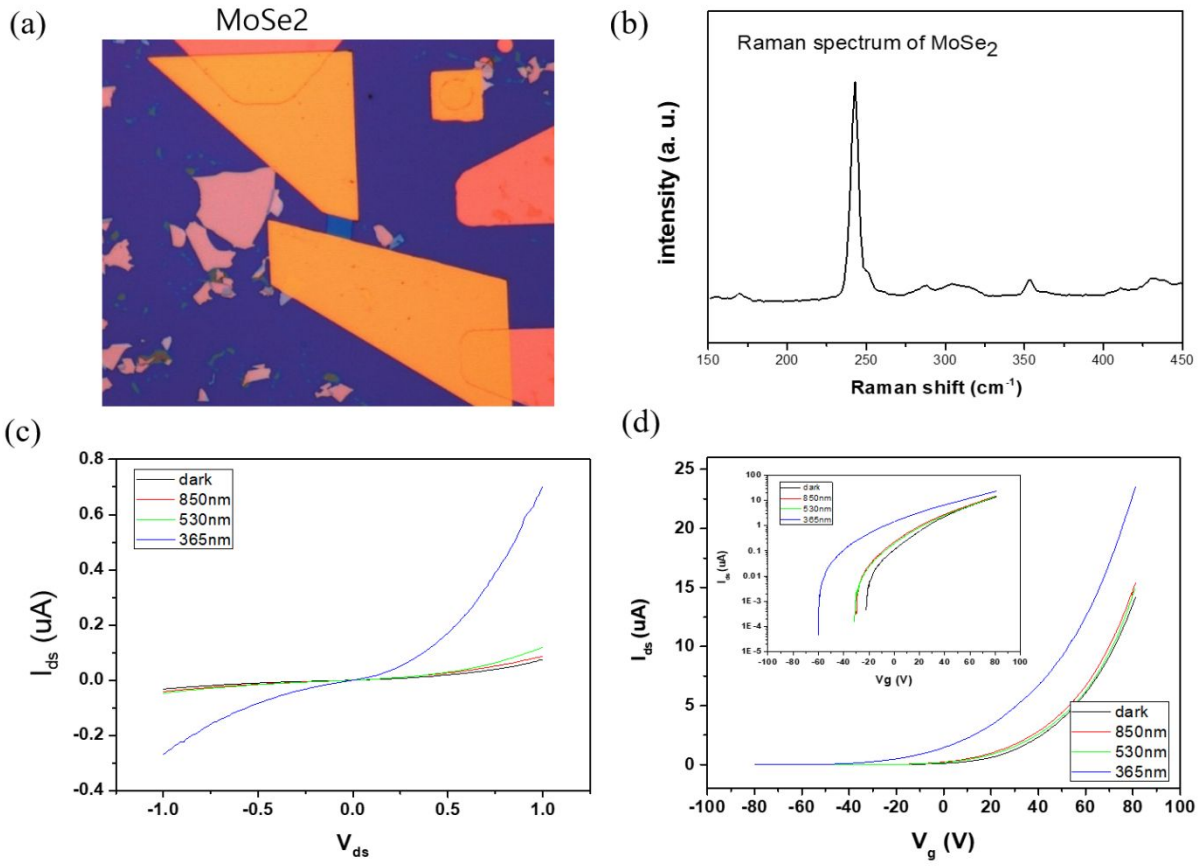

Figure S4 The optoelectronic data of few layer $MoSe_2$ based FET. (a) The optical microscopic image, (b) Raman spectra, (c) I-V curve at different illumination conditions, and (d) transfer curves depending on the back-gate voltage (@V_{ds} = 1 V). The inset is a semi-log plot of the same data.

To investigate the characteristics of $MoSe_2$, a FET device was fabricated, as shown in Fig. S4(a). From Raman spectrum shown in Fig. S4(b), the device was confirmed to have the thickness corresponding to 4 layer flake. The I-V curves at various illumination conditions were measured as shown in Fig. S4(c). Photocurrent of $MoSe_2$ was increased conspicuously when UV (365 nm) was illuminated. The transfer curve depending on the back gate voltage was measured in Fig. S4(d), where $MoSe_2$ was confirmed to be n-type.

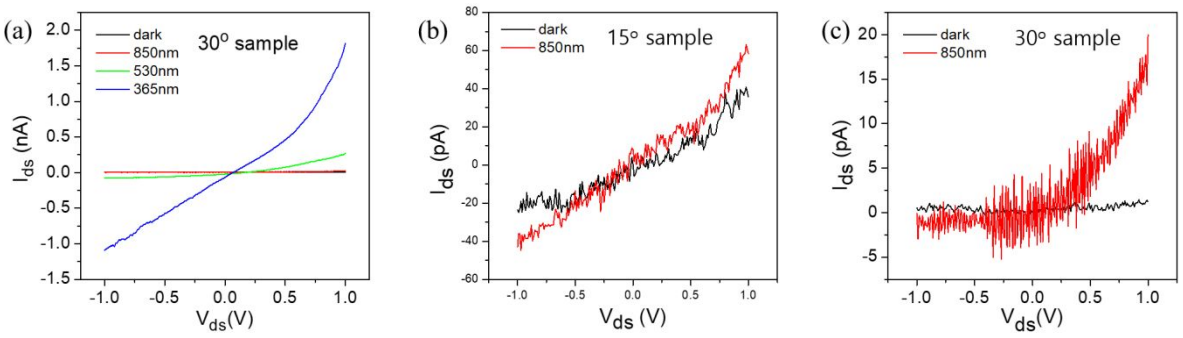

Figure S5 (a) I-V curve of heterostructure with twist angles 30˚ were measured under the LED illuminations as well as dark condition. For comparison, zoomed-in graphs of the I-V curves for dark and 850 nm conditions are shown for (b) 15˚ and (c) 30˚ HS devices, together.

I-V curve of HS with twist angles 30˚ was similar to that of the device with 15˚ as shown in Fig. S5(a). The diode-like behavior was weakened, due to weak coupling by the lattice mismatching. The photocurrent ($I_{ph} = I_{\text{illum}} - I_{\text{dark}}$) under 850 nm illumination was ~10 pA for both (b) 15˚ and (c) 30˚ HS devices in Fig. S5.

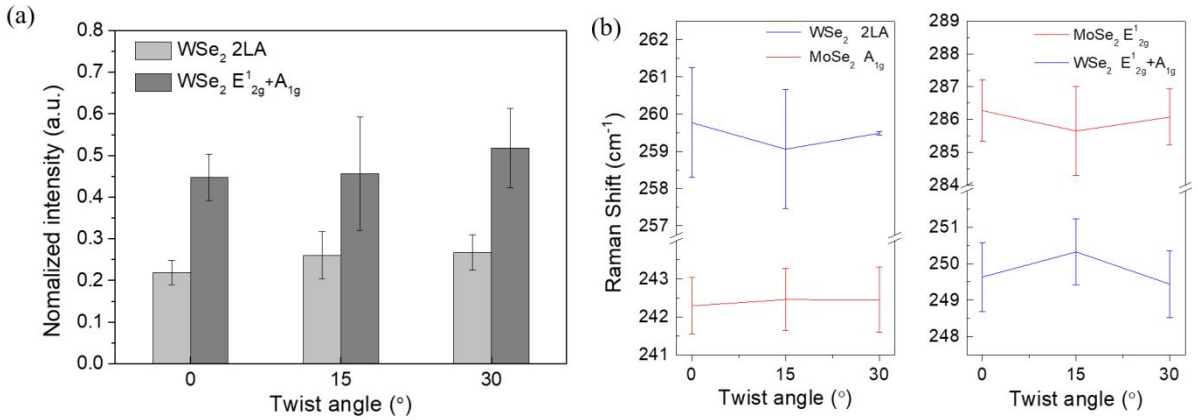

Figure S6 Raman signatures of $MoSe_2/WSe_2$ vertical heterostructures. (a) The normalized Raman intensities of A_{1g} and E^1_{2g} bands for WSe_2 in the HSs. (b) Raman shifts of A_{1g} and E^1_{2g} for WSe_2 and $MoSe_2$ versus twist angle in the HSs were plotted.

Figure S6 (a) shows a relative Raman peak intensities of A_{1g} and E^1_{2g} and 2LA modes for WSe_2 in the heterostructures with different twist angles. The raw data were normalized based on the background intensity, and it was averaged from 5 samples for each twist angle. The standard deviations were indicated as error bars. The Raman signals come from WSe_2 was strongest at the 30˚ sample and weakest at the 0˚ sample. Figure S6 (b) shows the positions of each major peak as a function of the twist angle, where the data were extracted from 5 samples for each angle. Though major changes were seen in the 15˚ sample, it is unclear whether this effect was directly due to the twist angle as the standard deviations (error bars) were wider than the variation of the average values.

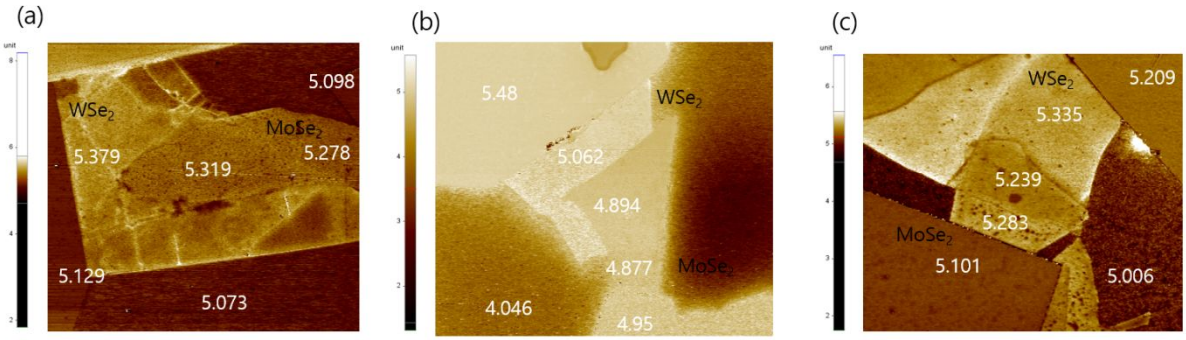

Sample # twist angle	0 : SiO_2	1 : Mo/Au	2 : W/Au	3 : $MoSe_2$	4 : WSe_2	5 : HS
Sample 1 (0°)	5.073	5.098	5.129	5.278	5.379	5.319
Sample 2 (15°)	4.046	4.95	5.48	4.877	5.062	4.894
Sample 3 (30°)	5.006	5.101	5.209	5.283	5.335	5.239

Unit (eV)

Figure S7 KPFM images and work function list. The samples with three different twist angles: (a) 0°, (b) 15°, and (c) 30°, were imaged and the work functions at the different regions are listed in the table.

The work functions for HS Φ_{HS} are close to that of $MoSe_2$, because it was measured on top of $MoSe_2$ layer by using Kelvin probe microscopy (KPFM), as shown in Fig. S7. Based on these results, the Fermi level of p-type WSe_2 is lower than that of n-type $MoSe_2$, and the energy bands for WSe_2 is shifted upward due to the band bending.

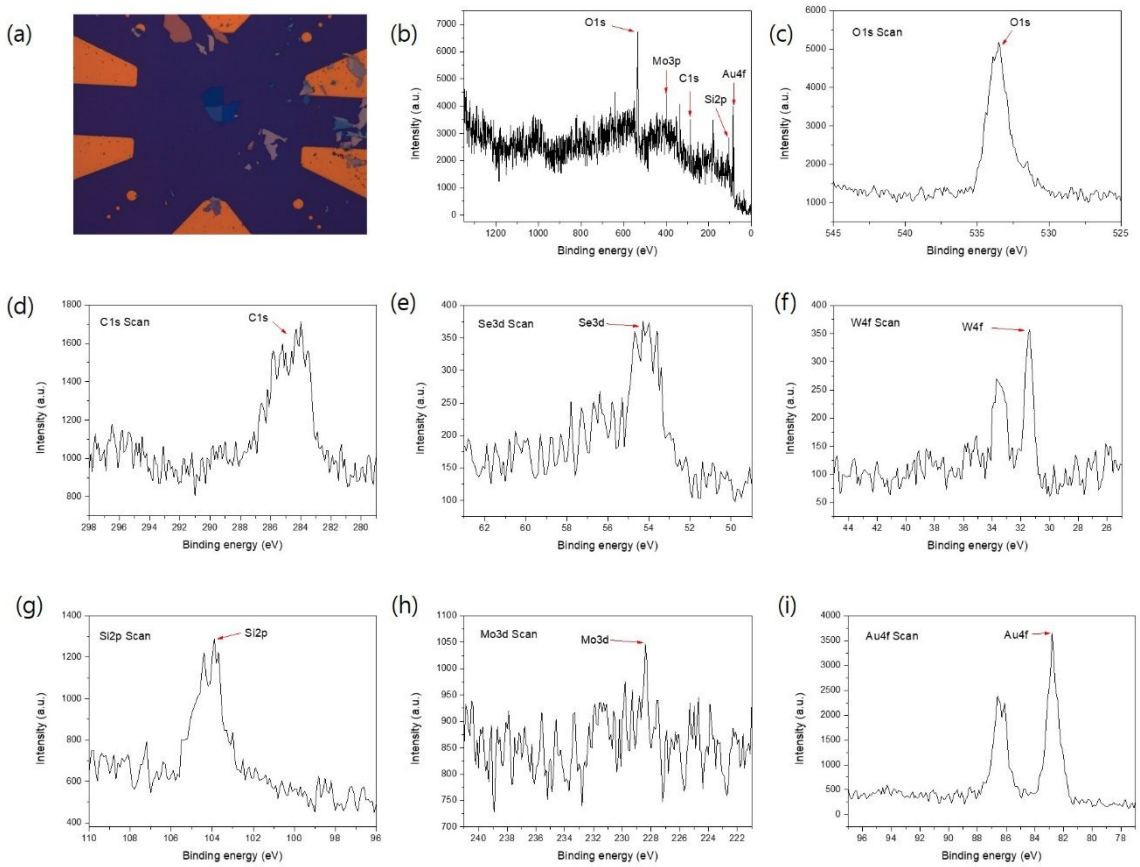

Figure S8 XPS full spectrum and each element spectrum of the MoSe2/WSe2 heterojunction sample. (a) An optical micrograph of the sample and (b) XPS full spectrum are shown together. High resolution spectra for (c) oxygen, (d) carbon, (e) selenium, (f) tungsten, (g) silicon, (h) molybdenum, and (i) gold were measured in detail.

We have performed the XPS measurement on the device, as shown in Fig. S8. (b) In the full spectrum, O, C, Se, W, Si, Mo, and Au were observed. As the spot size was larger than 15 μm, the data include the electrons from the electrode and substrate, as well as $MoSe_2$ and WSe_2. Thus, the peaks from Si, O, and Au appeared. (d) The carbon peak may be related with the contamination. In the carbon (C1s) spectrum, C-C bond (binding energy of 284.8 eV) was not observed strongly, meaning that there was a very small amount of polymer contamination based on carbon. (f) The spectrum for W (4f) shows two peaks, which is a typical spectrum for 2H structure of WSe_2 crystal. As the signal-to-noise ratio was not high enough, the data convolution analysis was not available. Judging from the raw data, the peak corresponding to 1T structure was not revealed. (h) The Mo (3d) spectrum shows a weak peak due to the small size of the $MoSe_2$ crystal, and further detailed analysis was not available.

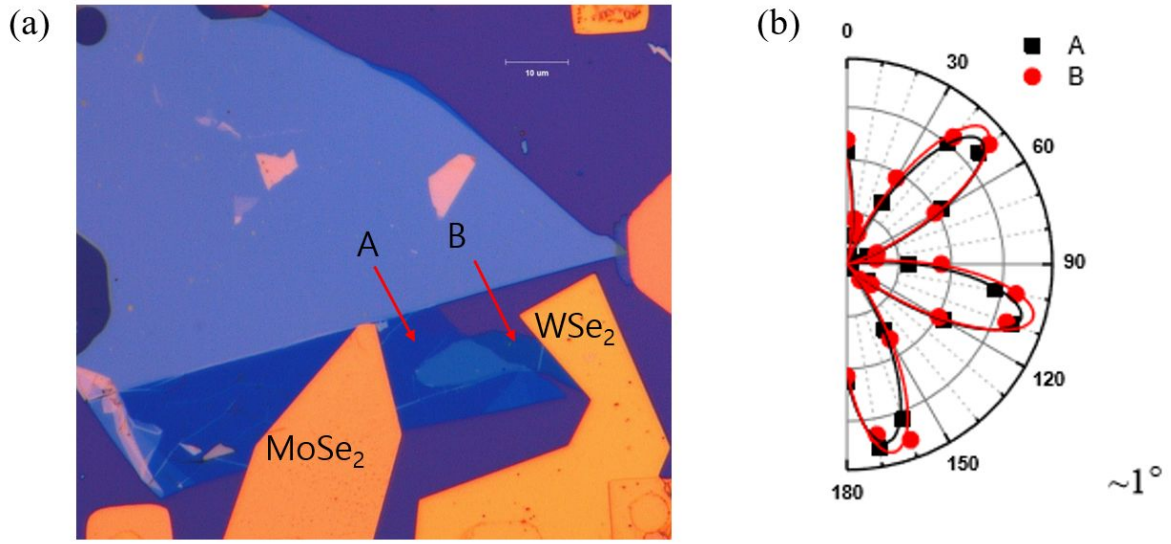

Figure S9. (a) Optical micrograph of a heterostructure device with the twist angle of 0° (b) A polar plot shows the second harmonic generation (SHG) intensity of $MoSe_2$ ('A') and WSe_2 ('B') labelled in (a).

From a sample fabricated with 0° twist angle by means of XRD, SHG data showed 1° angle difference between the $MoSe_2$ and WSe_2, as shown in Fig. S9. Considering the experimental error, it was confirmed that the twist angle was sustained in our fabrication process.

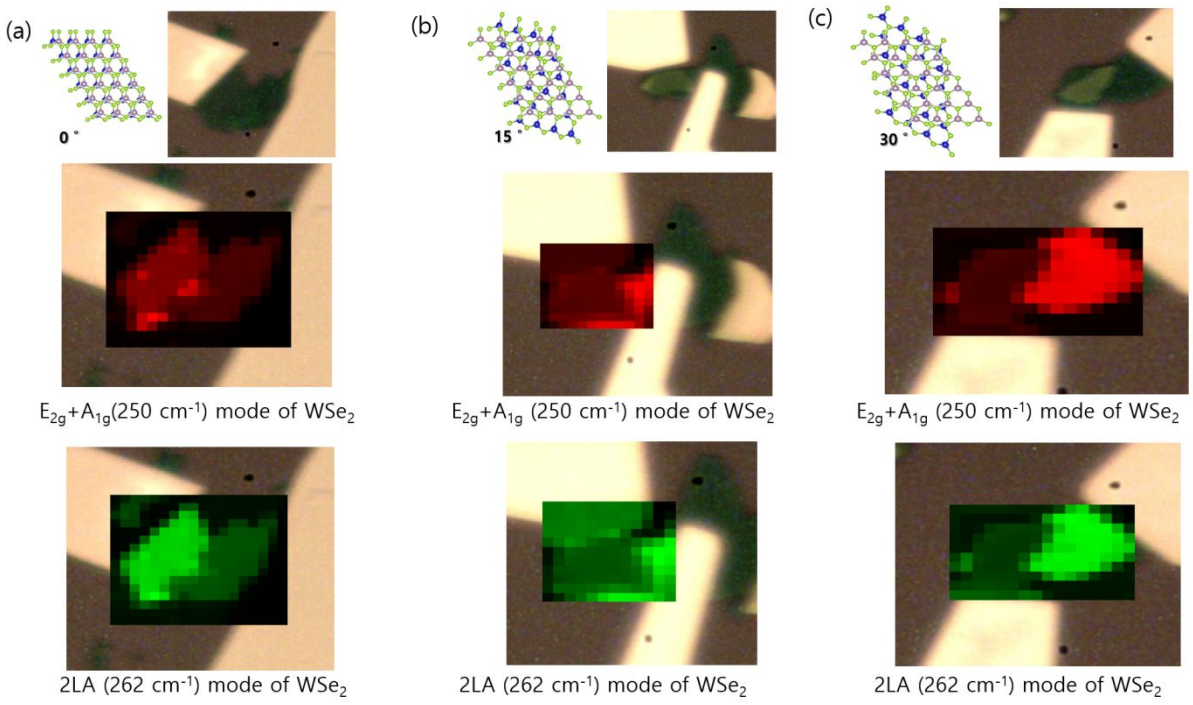

Figure S10 Raman mapping images of the WSe_2, $MoSe_2$, and $MoSe_2/WSe_2$ heterojunction for three samples with different twist angles: (a) 0^o, (b) 15^o, (c) 30^o.

The Raman mapping images of the WSe_2, $MoSe_2$, and $MoSe_2/WSe_2$ heterojunction are shown in Fig. S10. The intensities were mapped at the Raman shift positions of E^1_{2g} and A_{1g} (250 cm^{-1}) and 2LA (262 cm^{-1}) modes for WSe_2. In the mapping images, the intensity difference between $MoSe_2$ and WSe_2 are clear, but the overlapped areas are not much different from $MoSe_2$ region, because it was located in the top part.